Dynamic structure factor and momentum distribution of a trapped Bose gas

F. Zambelli,[1] L. Pitaevskii,[1,2] D. M. Stamper-Kurn,[3] and S. Stringari[1]
[1]*Dipartimento di Fisica, Università di Trento and Istituto Nazionale per la Fisica della Materia, I-38050 Povo, Italy*
[2]*Kapitza Institue for Physical Problems, 117334 Moscow, Russia*
[3]*Norman Bridge Laboratory of Physics, California Institute of Technology 12-33, Pasadena, California 91125*
(Received 7 December 1999; revised manuscript received 24 February 2000; published 16 May 2000)

The dynamic structure factor of a trapped Bose-Einstein condensed gas is investigated at zero temperature in the framework of Bogoliubov theory. Different values of momentum transfer are considered, ranging from the phonon to the single-particle regime. Various approximate schemes are discussed, including the local density approximation, where the system is locally described as a uniform gas, and the impulse approximation, in which the response is fixed by the momentum distribution of the condensate. A comprehensive approach, based on the eikonal expansion, is presented. The predictions of theory are successfully compared with the results of recent two-photon Bragg scattering experiments, at both low and high momentum transfer. Relevant features of the dynamic structure factor are also discussed using the formalism of sum rules and the concept of scaling. Particular emphasis is given to the regime of high momentum transfer, in which the dynamic structure factor is sensitive to the behavior of the order parameter in momentum space, and some instructive examples showing the consequence of long-range coherence are presented.

PACS number(s): 03.75.−b, 03.65.−w, 05.30.Jp, 32.80.−t

I. INTRODUCTION

The dynamic structure factor provides an important characterization of the dynamic behavior of quantum many-body systems. In particular, its exploration has played a crucial role in understanding the physics of superfluid ^{4}He, starting from the measurement of the roton spectrum [1] until the more recent determinations of the condensate fraction available from neutron scattering experiments [2]. The dynamic structure factor is measurable through inelastic scattering, in which the probe particle is weakly coupled to the many-body system so that the scattering may be described within the Born approximation [3]. In the case of dilute gases it can be measured via inelastic light scattering as recently shown by the experiments of Refs. [4,5] carried out on a trapped Bose gas of sodium atoms. The dynamic structure factor provides information on both the spectrum of collective excitations, which can be investigated at low momentum transfer, and the momentum distribution, which characterizes the behavior of the system at high momentum transfer, where the response is dominated by single-particle effects.

In superfluid helium the typical momentum giving the transition between the collective and the single-particle behavior is fixed by the inverse of the range of two-body forces, a value close to the average interatomic distance. At larger momenta one explores microscopic features of the system that are sensitive to short-range correlations and to the details of the two-body interaction. The situation is very different in a dilute gas where the transition takes place at momenta much smaller than the inverse of the scattering length, which fixes the range of interactions. As a consequence, in a Bose gas one can explore a domain of relatively high momenta, where the response of the system is not affected by collective features, nor by short-range correlations, but is determined by the momentum distribution of the condensate. While in a uniform system this distribution is a simple δ function, in a trapped gas it exhibits a nontrivial behavior and is strongly affected by the presence of two-body interactions.

The purpose of this paper is to provide a systematic theoretical discussion of the behavior of the dynamic structure factor of inhomogeneous Bose-Einstein condensates at zero temperature and to make quantitative comparisons with the recent data obtained with two-photon Bragg scattering experiments [4,5], pointing out the role of two-body interactions at both low and high momentum transfer. The applicability of both the local density (LDA) and of the impulse approximation (IA) will be discussed in detail. The LDA assumes that the system can be locally described as a uniform gas, and is adequate at moderately low values of momentum transfer. Conversely, in the IA the dynamic structure factor is sensitive to the momentum distribution, which, for Bose-Einstein condensed systems, is determined not locally but globally, according to the size and shape of the condensate wave function. A comprehensive description of both the LDA and IA regimes will be presented using the eikonal expansion, which holds in the single-particle regime at high momentum transfer. Special emphasis will be given to sum rules as well as to the scaling behavior exhibited by the dynamic structure factor in the IA regime. Finally we will point out the occurrence of interesting features exhibited by the dynamic structure factor in the presence of vortices and of interference effects in momentum space.

II. DYNAMIC STRUCTURE FACTOR AND BOGOLIUBOV THEORY

The dynamic structure factor of a many-body system is defined by the expression

$$S(\mathbf{q},E)=\frac{1}{\mathcal{Z}}\sum_{mn} e^{-\beta E_m}|\langle m|\rho_{\mathbf{q}}|n\rangle|^2\delta(E-E_m+E_n), \quad (1)$$

where $\mathbf{q}$ and E are the momentum and energy transferred by the probe to the sample. In Eq. (1) $|n\rangle$ and E_n are the eigenstates and eigenvalues of the Hamiltonian of the system, $e^{-\beta E_n}$ is the usual Boltzmann factor, $\rho_{\mathbf{q}}=\Sigma_j e^{i\mathbf{q}\cdot\mathbf{r}_j/\hbar}$ is the Fourier transform of the one-body density operator, and $\mathcal{Z}$ is the canonical partition function.

In Refs. [4,5], the dynamic structure factor of a trapped Bose-Einstein condensate is measured using two-photon optical Bragg spectroscopy. Two laser beams are impingent upon the condensate. The difference in the wave vectors of the beams defines the momentum transfer $\mathbf{q}$, and the frequency difference between the beams defines the energy transfer E. The atoms exposed to these beams can undergo a stimulated light scattering event by absorbing a photon from one of the beams and emitting into the other. After exposure to these laser beams, the response of the condensate is measured by a time-of-flight technique by which the number of optically excited atoms or, similarly, the net momentum transfer to the gas, can be determined. The momentum transfer in each of these experiments was fixed by the particular optical setup, while the energy transfer was scanned by varying the frequency difference between the beams. Because atoms could be scattered by absorbing a photon from either of the laser beams, the response of the system actually measures the combination $S(\mathbf{q},E)-S(-\mathbf{q},-E)$, thus significantly suppressing the effects of temperature in the measured signal.

Let us start our discussion by recalling that in an ideal uniform gas Eq. (1) takes the simple form [6]

$$S(\mathbf{q},E)=\sum_{\mathbf{p}} n_{\mathbf{p}}[1\pm n_{\mathbf{p}+\mathbf{q}}]\delta\left(E-\frac{(\mathbf{p}+\mathbf{q})^2}{2m}+\frac{p^2}{2m}\right), \quad (2)$$

where $n_{\mathbf{p}}=\langle a_{\mathbf{p}}^{\dagger}a_{\mathbf{p}}\rangle$ is the statistical average of the operator $a_{\mathbf{p}}^{\dagger}a_{\mathbf{p}}$, and the sign $+$ $(-)$ holds for Bose (Fermi) statistics. The scattering process is hence enhanced and suppressed in Bose and Fermi gases, respectively. In the fermionic case this reflects the Pauli exclusion principle. For large momentum transfer $\mathbf{q}$ the exchange term of Eq. (2) is negligible because the momentum distribution decreases rapidly at high momenta and, making the usual replacement $\Sigma_{\mathbf{p}}\rightarrow V/h^3\int d\mathbf{p}$, one finds the expression

$$S_{IA}(\mathbf{q},E)=\int d\mathbf{p}\,\delta\left(E-\frac{(\mathbf{p}+\mathbf{q})^2}{2m}+\frac{p^2}{2m}\right)n(\mathbf{p}), \quad (3)$$

known as the impulse approximation (IA) [7]. In Eq. (3)

$$n(\mathbf{p})=\langle\hat{\psi}(\mathbf{p})^{\dagger}\hat{\psi}(\mathbf{p})\rangle \quad (4)$$

is the momentum distribution of the system, $\hat{\psi}(\mathbf{p})=(2\pi\hbar)^{-3/2}\int d\mathbf{r}\hat{\psi}(\mathbf{r})e^{i\mathbf{p}\cdot\mathbf{r}/\hbar}$ being the Fourier transform of the field operator. For uniform systems occupying a volume V the momentum distribution is related to the occupation number entering Eq. (2) by $n(\mathbf{p})=Vn_{\mathbf{p}}/h^3$. It is important to stress that the validity of Eq. (3) is not restricted to the ideal gas, but holds in general at high momentum transfer also for interacting and nonuniform systems, independent of quantum statistics. Of course in this case the momentum distribution $n(\mathbf{p})$ will differ significantly from that of the ideal gas.

At small momentum transfer the ideal gas prediction (2) is inadequate, especially in the case of Bose gases, in which mean field interactions drastically modify the structure of $S(\mathbf{q},E)$, giving rise to the propagation of phonons.

The calculation of $S(\mathbf{q},E)$ in interacting many-body systems requires in general a major theoretical effort. In the following we will limit ourselves to the $T=0$ case and to the study of dilute Bose gases where Bogoliubov theory is applicable. This restricts the range of momenta q to the ''macroscopic'' regime $qa\ll\hbar$ where a is the s-wave scattering length. For larger values of q short-range correlations become important and Bogoliubov theory is no longer adequate. In the conditions of the experiment of [4], carried out on a gas of sodium atoms, the Bogoliubov approach is well applicable since $q/\hbar\sim 20\ \mu\mathrm{m}^{-1}$ and $qa\sim 0.06\hbar$. The macroscopic condition is even better satisfied in the experiment of [5] where smaller values of q have been used.

According to Bogoliubov theory the excited states of the system are given by the solution of the coupled equations [8]

$$\epsilon u(\mathbf{r})=\left[-\frac{\hbar^2}{2m}\nabla^2+V_{\mathrm{ext}}(\mathbf{r})-\mu+2g\psi_0^2(\mathbf{r})\right]u(\mathbf{r})+g\psi_0^2(\mathbf{r})v(\mathbf{r}), \quad (5)$$

$$-\epsilon v(\mathbf{r})=\left[-\frac{\hbar^2}{2m}\nabla^2+V_{\mathrm{ext}}(\mathbf{r})-\mu+2g\psi_0^2(\mathbf{r})\right]v(\mathbf{r})+g\psi_0^2(\mathbf{r})u(\mathbf{r}) \quad (6)$$

for the ''particle'' and ''hole'' components of the elementary modes. In Eqs. (5) and (6) ϵ is the energy of the excitation, and $V_{\mathrm{ext}}(\mathbf{r})$ is the external potential for which, unless differently specified, we make the axially symmetric harmonic choice:

$$V_{\mathrm{ext}}(\mathbf{r})=\frac{1}{2}m\omega_{\perp}^2(x^2+y^2)+\frac{1}{2}m\omega_z^2z^2. \quad (7)$$

Furthermore μ is the chemical potential, $g=4\pi\hbar^2a/m$ is the coupling constant, which will be assumed to be positive, and finally $\psi_0(\mathbf{r})$ is the order parameter characterizing the ground state of the system.

In terms of the functions $u_n(\mathbf{r})$ and $v_n(\mathbf{r})$, which satisfy the orthonormalization condition [9]

$$\int d\mathbf{r}[u_n^*(\mathbf{r})u_m(\mathbf{r})-v_n^*(\mathbf{r})v_m(\mathbf{r})]=\delta_{nm}, \quad (8)$$

the relevant matrix element of the density operator takes the form

$$\langle n|\rho_{\mathbf{q}}|0\rangle=\int d\mathbf{r}[u_n^*(\mathbf{r})+v_n^*(\mathbf{r})]e^{i\mathbf{q}\cdot\mathbf{r}/\hbar}\psi_0(\mathbf{r}) \quad (9)$$

and the dynamic structure factor then becomes, at $T=0$, [10]

$$S(\mathbf{q},E)=\sum_n\left|\int d\mathbf{r}[u_n^*(\mathbf{r})+v_n^*(\mathbf{r})]e^{i\mathbf{q}\cdot\mathbf{r}/\hbar}\psi_0(\mathbf{r})\right|^2\delta(E-\epsilon_n). \quad (10)$$

In the case of a uniform gas the ''particle'' and ''hole'' components are plane waves: $u(\mathbf{r})=U\exp(i\mathbf{p}\cdot\mathbf{r}/\hbar)$ and $v(\mathbf{r})=V\exp(i\mathbf{p}\cdot\mathbf{r}/\hbar)$ and the coupled equations (5)–(6) give rise to the Bogoliubov excitation spectrum [11]:

$$\epsilon(p)=\sqrt{\frac{p^2}{2m}\left(\frac{p^2}{2m}+2gn\right)}, \tag{11}$$

where n is the density of the gas. This spectrum exhibits a phonon dispersion $\epsilon=cp$ at low momenta, with the velocity of sound given by $c=\sqrt{gn/m}$, while in the opposite limit of high momenta it approaches the free particle energy $\epsilon=p^2/2m$. The transition between the collective and the single-particle behavior occurs at momenta of the order of $\hbar/\xi$, where

$$\xi=\frac{1}{\sqrt{8\pi na}} \tag{12}$$

is the so-called healing length.

Using the normalization condition (8), one finds the result

$$S_B(\mathbf{q},E)=N\frac{q^2}{2m\epsilon(q)}\delta(E-\epsilon(q)) \tag{13}$$

for the dynamic structure factor, which consists of a δ function centered at the Bogoliubov frequency (11). Equation (13) yields the Feynman-like result

$$S_B(\mathbf{q})=\frac{1}{N}\int dES(\mathbf{q},E)=\frac{q^2}{2m\epsilon(q)} \tag{14}$$

for the static structure factor, which tends linearly to zero at low momenta, and saturates to 1 in the opposite, high-q limit.

Results (13) and (14) hold for uniform Bose gases. In the presence of nonuniform trapping a natural generalization is provided by the local density approximation (LDA). For large condensates, where the density profile varies in a smooth way, the system behaves locally as a piece of uniform gas whose dynamic structure factor is given by the expression (13), evaluated at the corresponding density [12]:

$$S_{LDA}(\mathbf{q},E)=\int d\mathbf{r}\, n(\mathbf{r})\,\delta(E-\epsilon(\mathbf{r},\mathbf{q}))\frac{q^2}{2m\epsilon(\mathbf{r},\mathbf{q})}. \tag{15}$$

In Eq. (15) $n(\mathbf{r})$ is the ground state density of the system, and $\epsilon(\mathbf{r},\mathbf{q})=\epsilon(n(\mathbf{r}),\mathbf{q})$ is the local Bogoliubov dispersion (11). Equation (15) is expected to describe accurately the dynamic structure factor for momenta larger than $\hbar/R$ where R is the radius of the condensate, since the effects of discretization in the excitation spectrum can be safely ignored. In the case of deformed traps we will always consider situations where q is larger than both $\hbar/R_\perp$ and $\hbar/R_z$, where $R_\perp$ and R_z are the radial and axial sizes. Actually in the experiments of Ref. [5] these conditions are well satisfied. At the same time the momentum transfer q should not be too large since the local density approximation ignores the Doppler effect associated with the spreading of the momentum distribution of the condensate, which is expected to become the leading effect in the dynamic structure factor at very large values of q. The Doppler broadening is accounted for by the impulse approximation (3), which, however, ignores the mean field effects of Bogoliubov theory. The conditions of applicability for both LDA and IA will be established in the next section.

III. LOCAL DENSITY, IMPULSE, AND EIKONAL APPROXIMATIONS

In Sec. II we introduced two useful approximations to the dynamic structure factor of an interacting Bose gas: the impulse (3) and local density (15) approximations. These two descriptions hold in different regimes of momentum transfer. The purpose of this section is to discuss the corresponding predictions and conditions of applicability. We will also present a comprehensive description of the high-q response of the system, based on eikonal expansion, which includes the LDA and the IA as special cases.

A. Local density approximation

Let us first discuss the local density approximation (15). An explicit expression for $S(\mathbf{q},E)$ can be obtained working in the Thomas-Fermi limit $Na/a_{\rm ho}\gg 1$, where the ground state density is given by (see, for example, [13])

$$n(\mathbf{r})=\frac{1}{g}[\mu-V_{\rm ext}(\mathbf{r})], \tag{16}$$

and the chemical potential takes the form

$$\mu=\frac{1}{2}\left(15\frac{Na}{a_{\rm ho}}\right)^{2/5}\hbar\omega_{\rm ho}. \tag{17}$$

In Eq. (17) $a_{\rm ho}=\sqrt{\hbar/m\omega_{\rm ho}}$ is the oscillator length calculated using the geometrical average $\omega_{\rm ho}=(\omega_\perp^2\omega_z)^{1/3}$ of the oscillator frequencies. Using this density profile and the result of Eq. (11) for the excitation spectrum, one obtains $S(\mathbf{q},E)$ for a trapped Bose condensate as [12,5]:

$$S_{LDA}(\mathbf{q},E)=\frac{15}{8}\frac{(E^2-E_{\rm r}^2)}{E_{\rm r}\mu^2}\sqrt{1-\frac{(E^2-E_{\rm r}^2)}{2E_{\rm r}\mu}}, \tag{18}$$

where

$$E_{\rm r}=\frac{q^2}{2m} \tag{19}$$

is the recoil energy. Different from the case of a uniform gas [see Eq. (13)], the dynamic structure factor is no longer a δ function, its value being different from zero in the interval $E_{\rm r}<E<E_{\rm r}\sqrt{1+2\mu/E_{\rm r}}$. The value $E=E_{\rm r}$ corresponds to the excitation energy in the region near the border where the gas is extremely dilute and hence noninteracting. The value $E=E_{\rm r}\sqrt{1+2\mu/E_{\rm r}}$ is the excitation energy of a Bogoliubov gas evaluated at the central density. Notice that the LDA expression (18) for $S(\mathbf{q},E)$ does not depend on the direction of the vector $\mathbf{q}$ even in the presence of a deformed trap.

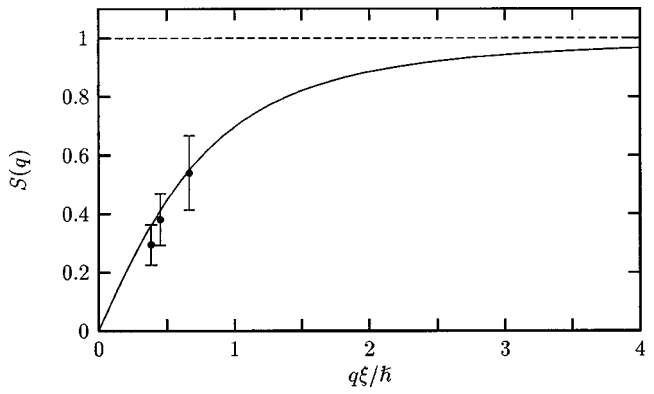

FIG. 1. Static structure factor $S(q)$ at $T=0$ as a function of $q\xi/\hbar$. The prediction (20) of the local density approximation (solid line) is compared with the experimental points taken from [5]. The result of the noninteracting model (dashed line) is also indicated.

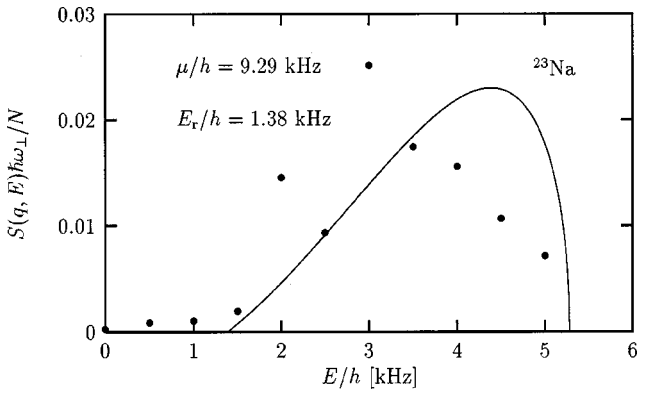

FIG. 2. Dynamic structure factor calculated using the local density approximation (18). Experimental points are taken from Ref. [5]. The trapping frequencies are $\omega_\perp = 2\pi 150$ Hz and $\omega_z = 2\pi 18$ Hz.

As pointed out in the previous section, the local density approximation requires that the momentum transfer be larger than $\hbar/R$. For smaller values of q the response of the system is sensitive to the discretized modes of the system and the LDA cannot be longer employed. The theoretical analysis of the dynamic structure factor in this regime of low momentum transfer has been carried out in [10]. In the following we will always assume that the condition $q \gg \hbar/R$ is satisfied.

Starting from (18) one can evaluate the inelastic static structure factor $S(\mathbf{q}) = N^{-1}\int S(\mathbf{q},E)dE$, which takes the analytic form [5]:

$$S(q) = \frac{15}{4}\left\{ \frac{3+\alpha}{4\alpha^2} - \frac{(3+2\alpha-\alpha^2)}{16\alpha^{5/2}}\left[\pi + 2\arctan\left(\frac{\alpha-1}{2\sqrt{\alpha}} \right) \right] \right\}, \tag{20}$$

with $\alpha = 2\mu/E_r$. When $q\xi \ll \hbar$, Eq. (20) behaves like $S(q) \sim q/(2m\bar{c})$, reflecting the role played by dynamic correlations, which strongly suppress light scattering in the phonon regime (see Fig. 1). Here $\bar{c} = 32\sqrt{\mu/m}/15\pi$ corresponds to an average sound velocity, which, as expected, is smaller than the value $\sqrt{\mu/m}$ calculated in the center of the trap.

Useful information about the dynamic structure factor can be obtained by evaluating its energy moments $m_k(\mathbf{q}) = \int_{0^+}^{\infty} E^k S(\mathbf{q},E)dE$. For example, the average excitation energy $\bar{E}$ and the rms width $\Delta_{\rm rms}$ can be defined as

$$\bar{E} = \frac{m_1}{m_0}, \tag{21}$$

and

$$\Delta_{\rm rms} = \sqrt{\frac{m_2}{m_0} - \left(\frac{m_1}{m_0} \right)^2}, \tag{22}$$

respectively.

Let us first discuss the phonon regime in which $E_r \ll \mu$, or, equivalently, $q\xi \ll \hbar$, where ξ is the healing length (12) calculated at the central density. Typical values of ξ in sodium samples, where $a = 2.75$ nm, are of 0.1–1 μm depending on the density of the gas. Using the LDA expression (18) for $S(\mathbf{q},E)$ one finds, in the phonon regime, the results $\bar{E} = \bar{c}q$ and $\Delta_{\rm rms} \simeq 0.3\bar{c}q$, showing that the width of the signal is not much smaller than the average energy. The shape of $S(\mathbf{q},E)$ turns out to be asymmetric as a function of E (see Fig. 2), and the peak response occurs at an energy that is higher (by about 15%) than $\bar{E}$.

The dynamic structure factor $S(\mathbf{q},E)$ has been recently measured in the phonon regime [5]. A typical experimental curve is reported in Fig. 2 together with the prediction (18). These measurements also show (see Fig. 1) the static structure factor $S(q)$ in the phonon regime to be smaller than the noninteracting gas value $S(q)=1$, in agreement with the predictions of Eq. (20) [14].

In the opposite limit of large momentum transfer, where $q\xi \gg \hbar$, the excitation energy (21) predicted by the LDA is given by the expression

$$\bar{E} = E_r + \frac{4}{7}\mu. \tag{23}$$

This result corresponds to the average of the Bogoliubov energy $\epsilon(\mathbf{q},\mathbf{r}) = q^2/2m + gn(\mathbf{r})$ holding at high q. Notice that, due to the asymmetric shape of the dynamic structure factor (18), the average energy (23) turns out to be smaller than the peak energy

$$E_{\rm peak} = E_r + \frac{2}{3}\mu. \tag{24}$$

This asymmetry should be, in principle, taken into account in the fit of experimental data. However, the shift of the line center was effectively determined from experiments in [4] using symmetric Gaussian fits and was in good agreement with Eq. (23) (see Fig. 3). In the same regime of large q the rms width predicted by the LDA is given by

$$\Delta_{LDA} = \sqrt{\frac{8}{147}}\mu \tag{25}$$

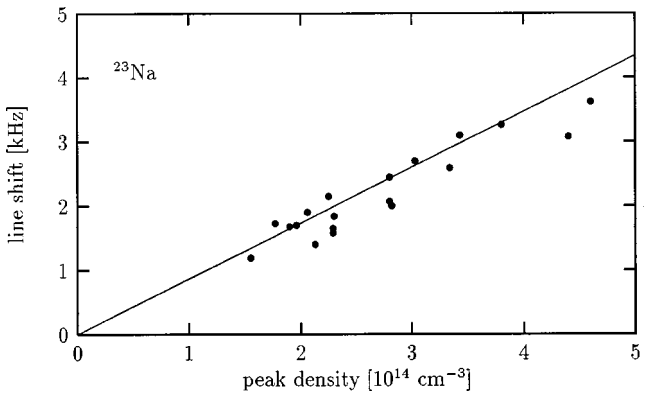

FIG. 3. Line shift as a function of the central density of the cloud. The straight line is the theoretical prediction (23), and the circles are the experimental points of Ref. [4].

and is independent of q. In relating these theoretical results to experimental data, it is worth noting that the experimental data are further broadened by the finite duration of the laser pulses, which would tend to make the spectra less asymmetric (see also Fig. 5).

Thus, for momentum transfers q which are sufficiently small to allow the use of the local density approximation, the structure factor of an inhomogeneous Bose-Einstein condensate can be derived from the Bogoliubov spectrum for a uniform condensed gas. Studies in this regime therefore serve as a probe of the spectrum of both collective ($q\xi \ll \hbar$) and free-particle ($q\xi \gg \hbar$) excitations.

B. Impulse approximation

Let us now discuss the response of a trapped condensate to very large momentum transfers at which the form of the dynamic structure factor is dominated by Doppler broadening. In this regime, the dynamic structure factor is correctly described by the impulse approximation (3). Inelastic scattering at such high momentum transfers allows one to directly measure the momentum distribution of a trapped Bose gas. The possibility of such measurements is highly appealing since most of experimental investigations in these systems have been so far limited to the study of density profiles. In current experiments on harmonically confined Bose gases, the sizes of the condensate R and of the thermal cloud R_T are typically comparable. In the Thomas-Fermi regime, the ratio between the two radii is given as

$$\frac{R}{R_T} \sim \sqrt{\frac{\mu}{k_B T}} = \sqrt{\frac{\hbar \omega_{\rm ho}}{k_B T}} \left(15 \frac{N_0 a}{a_{\rm ho}} \right)^{1/5}, \tag{26}$$

where N_0 is the number of atoms in the condensate. Due to the large value of the Thomas-Fermi parameter $N_0 a/a_{\rm ho}$, this ratio is typically close to unity. Expression (26) also provides an estimate for the ratio of sizes of the two components measured in time-of-flight experiments, in which the trap is suddenly switched off and the gas allowed to freely expand. While the expansion of the thermal cloud is indicative of the noncondensate momentum distribution before release from the trap, the expansion of the condensate in the Thomas-Fermi regime is dominated by the release of interaction energy and does not reveal its initial momentum distribution.

In contrast, the distinction between the condensate and the thermal cloud in momentum space is stark. A confined condensate of finite size has a momentum distribution of width $\Delta p_c \sim \hbar/R$ fixed by the inverse of the size R of the condensate. The momentum width of the thermal cloud is instead given by the temperature of the gas as $\Delta p_T \sim \sqrt{m k_B T}$. For harmonic confinement in the Thomas-Fermi regime, one then finds

$$\frac{\Delta p_c}{\Delta p_T} \sim \sqrt{\frac{\hbar \omega_{\rm ho}}{k_B T}} \left(15 \frac{N_0 a}{a_{\rm ho}} \right)^{-1/5}. \tag{27}$$

In contrast with the comparison of the condensate and the thermal cloud in coordinate space (26), the distinction between the two components in momentum space is strongly *enhanced* by two body interactions as the Thomas-Fermi parameter $N_0 a/a_{\rm ho}$ increases. The investigation of the momentum distribution consequently provides a deeper understanding of the phenomenon of BEC. In particular the smallness of the width Δp_c reflects the presence of long-range coherence. Measuring the momentum distribution at zero temperature would, in principle, give access also to the quantum depletion of the condensate. In practice, however, the quantum depletion is too small and broadened over too large a momentum range [15] to be observable in present experiments.

The expression (3) for the impulse approximation can be also written in the form

$$S_{IA}(\mathbf{q},E) = \frac{m}{q} \int dp_y dp_z n(p_x, p_y, p_z), \tag{28}$$

where we have assumed that the vector $\mathbf{q}$ is oriented along the x axis, and $p_x = m(E - E_{\rm r})/q$. The integral $\int dp_y dp_z n(p_x, p_y, p_z)$ is also called the longitudinal momentum distribution. Equations (3) and (28) show that in the regime of applicability of the IA one can extract useful information on the momentum distribution starting from the experimental measurement of the dynamic structure factor.

In a dilute Bose gas at zero temperature the momentum distribution is given by $n(\mathbf{p}) = |\phi(\mathbf{p})|^2$, where

$$\phi(\mathbf{p}) = (2\pi\hbar)^{-3/2} \int d\mathbf{r} \psi(\mathbf{r}) e^{i\mathbf{p}\cdot\mathbf{r}/\hbar} \tag{29}$$

is the Fourier transform of the order parameter. The form of $n(\mathbf{p})$ for a trapped condensate has been discussed previously [16,17]. In the Thomas-Fermi limit $Na/a_{\rm ho} \gg 1$ one finds the simple analytic result

$$n_{\rm TF}(\mathbf{p}) = N \frac{15}{16\lambda} \left(\frac{R_\perp}{\hbar} \right)^3 \left[\frac{J_2(\tilde{p})}{\tilde{p}^2} \right]^2, \tag{30}$$

where $J_2(z)$ is the usual Bessel function of order 2,

$$R_\perp = \left(15 \frac{Na}{a_{\rm ho}} \right)^{1/5} \lambda^{1/3} a_{\rm ho} \tag{31}$$

is the Thomas-Fermi radius of the condensate in the x-y plane, and $\tilde{p}=\sqrt{p_x^2+p_y^2+(p_z/\lambda)^2}R_\perp/\hbar$ is a dimensionless variable, with the parameter $\lambda=\omega_z/\omega_\perp$ fixing the anisotropy of the external potential.

Equation (30) explicitly shows that the momentum distribution scales as $1/R_\perp$ and is consequently much narrower than that of the noninteracting gas

$$n_{\mathrm{IBG}}(\mathbf{p})=N\left(\frac{a_{\mathrm{ho}}}{\hbar\sqrt{\pi}}\right)^3\exp\left[-\frac{a_{\mathrm{ho}}^2}{\hbar^2}\lambda^{1/3}\left(p_x^2+p_y^2+\frac{p_z^2}{\lambda}\right)\right], \tag{32}$$

since $R_\perp \gg a_{\mathrm{ho}}$.

In the impulse approximation (28) the peak of $S(\mathbf{q},E)$ coincides with the recoil energy E_{r}, while the curve is broadened due to the Doppler effect in the momentum distribution. A useful estimate of the broadening can be obtained carrying out a Gaussian expansion in the dynamic structure factor (28) near the peak value $E=E_{\mathrm{r}}$. One finds

$$S_{IA}(\mathbf{q},E)\simeq S_{IA}(\mathbf{q},E_{\mathrm{r}})\exp\left[-\frac{(E-E_{\mathrm{r}})^2}{2\Delta_{IA}^2}\right], \tag{33}$$

with $\Delta_{IA}^2=-[S_{IA}(\mathbf{q},E)/\partial_E^2 S_{IA}(\mathbf{q},E)]|_{E=E_{\mathrm{r}}}$. By calculating the second derivative of (28) with the Thomas-Fermi profile (30) for the momentum distribution, we obtain, after some straightforward algebra, the result

$$\Delta_{IA}=\sqrt{\frac{8}{3}}\frac{q\hbar}{mR_\perp}. \tag{34}$$

The Gaussian profile (33) reproduces very well the exact curve (see Fig. 6), so that the Doppler width (34) can be usefully compared with experiments, where the widths are usually extracted through Gaussian fits to the measured signal. The Doppler width (34) is linear in q, and for large momentum transfer it can become comparable to or even larger than the mean field width (25). In Fig. 4 we show the theoretical prediction (34) together with the experimental values obtained at several densities. This figure confirms that the IA accounts for the observed widths in the low density regime. At higher density the mean field effect (25) can no longer be neglected.

It is worth noticing that the width (34) should not be confused with the rms width (22), which requires the evaluation of the m_2 moment and, using the IA expression (3) or (28), takes the form

$$\Delta_{\mathrm{rms}}=q\sqrt{\frac{2}{m}E_{\mathrm{kin}}^x}, \tag{35}$$

instead of (34). Here $E_{\mathrm{kin}}^x=\int d\mathbf{p}p_x^2 n(\mathbf{p})/2m$ is the x component of the kinetic energy of the condensate. The evaluation of the kinetic energy requires a careful analysis [18,19] of the region near the boundary of the condensate, and cannot be evaluated using the Thomas-Fermi expression (30) for $n(\mathbf{p})$, which incorrectly yields a divergent result. For large N samples one finds [18], assuming isotropic trapping,

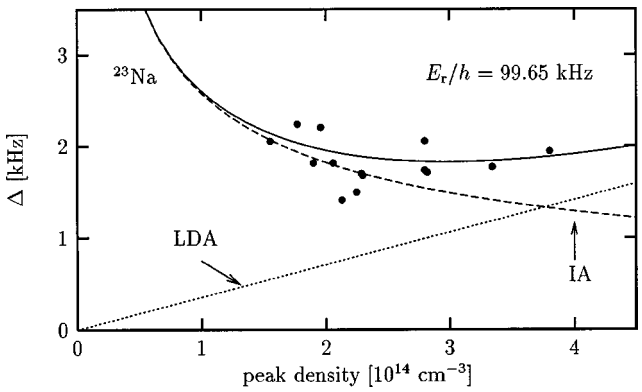

FIG. 4. Line width as a function of the central density of the sample. The solid line is the prediction of the eikonal approximation (43). The dashed and dotted lines correspond to the IA and LDA predictions (34) and (25), respectively. The theoretical results are compared with the experimental data of [4]. Both the eikonal and the experimental values are obtained through the Gaussian fit $S(q,\overline{E})\exp[(E-\overline{E})^2/2\Delta^2]$ to the signal. The momentum transfer is taken along the x axis. The trapping frequencies are $\omega_\perp=2\pi 195$ Hz and $\omega_z=2\pi 17$ Hz.

$$\frac{E_{\mathrm{kin}}^x}{N}\simeq\frac{5\hbar^2}{6mR^2}\ln\left(\frac{R}{1.3a_{\mathrm{ho}}}\right). \tag{36}$$

The logarithmic term reflects the fact that the m_2 moment, and hence the rms width, is sensitive to the high energy tails of the dynamic structure factor, a region which is difficult to measure since the intensity of the signal in the tails is very small. Because of this, estimate (34) is much more significant from the experimental point of view than expression (35).

The investigation of the dynamic structure factor also provides information on the coherence effects exhibited by the system and in particular on the behavior of the off-diagonal one-body density

$$\begin{aligned}\rho^{(1)}(\mathbf{s})&=N\int d\mathbf{R}d\mathbf{r}_2\cdots d\mathbf{r}_N\psi^*\left(\mathbf{R}+\frac{\mathbf{s}}{2},\mathbf{r}_2,\ldots,\mathbf{r}_N\right)\\&\quad\times\psi\left(\mathbf{R}-\frac{\mathbf{s}}{2},\mathbf{r}_2,\ldots,\mathbf{r}_N\right)\\&=\int d\mathbf{p}n(\mathbf{p})\exp\left[-i\frac{\mathbf{p}\cdot\mathbf{s}}{\hbar}\right],\end{aligned} \tag{37}$$

where $\psi(\mathbf{r}_1,\ldots,\mathbf{r}_N)$ is the many-body wave function of the system, and $n(\mathbf{p})$ is the momentum distribution. By taking the Fourier transform of Eq. (28) with respect to p_x, one finds the result

$$\rho^{(1)}(s_x,0,0)=\int dES_{IA}(\mathbf{q},E)\exp\left[-i\frac{ms_x}{\hbar q}(E-E_{\mathrm{r}})\right], \tag{38}$$

which shows that the one-body density is a measurable quantity if one works at high q where $S(\mathbf{q},E)\sim S_{IA}(\mathbf{q},E)$. In a uniform Bose-Einstein gas $\rho^{(1)}(s_x,0,0)$ tends to a constant

when s_x is large. In a finite system $\rho^{(1)}(s_x,0,0)$ always tends to zero when $s_x \to \infty$. The typical length over which $\rho^{(1)}$ decreases can be of the order of the size of the sample or smaller depending on the degree of coherence. Using, for example, the Gaussian profile (33) for $S(\mathbf{q},E)$ one finds

$$\rho^{(1)}(s_x,0,0) \sim N \exp\left[-\frac{s_x^2}{2\chi_x^2} \right], \tag{39}$$

with $\chi_x = R_\perp \sqrt{3/8}$. One can see from Eq. (39) that χ_x plays the role of a coherence length [20], which turns out to be of the order of the size of the system. This result reflects the fact that in a Bose-Einstein condensate the Heisenberg inequality $\Delta R \Delta p_c \geqslant \hbar/2$ is close to an identity.

C. Eikonal expansion

In order to describe the transition between the LDA and IA regimes discussed above and to better understand the corresponding conditions of applicability, it is useful to evaluate the high energy solutions of the Bogoliubov equations (5)–(6) using an eikonal expansion [21,22]. In the large q limit, where we are interested in the solutions with energy ϵ much larger than the chemical potential μ, one can neglect the function $v(\mathbf{r})$ in Eq. (5) and look for a solution of the form $u(\mathbf{r}) = \exp[i\mathbf{p}_f \cdot \mathbf{r}/\hbar]\tilde{u}(\mathbf{r})$, where $\mathbf{p}_f$ is the momentum of the excitation and $\tilde{u}(\mathbf{r})$ is a slowly varying function. Keeping only terms with first spatial derivative of $\tilde{u}(\mathbf{r})$ (eikonal approximation), the solution of (5) with energy $\epsilon = p_f^2/2m$ takes the form

$$u(\mathbf{r}) \simeq \exp\left[i \frac{\mathbf{p}_f \cdot \mathbf{r}}{\hbar} \right] \exp\left[-i \frac{m}{p_f \hbar} \int_0^x dx' V_{\mathrm{eff}}(x',y,z) \right], \tag{40}$$

where the effective potential $V_{\mathrm{eff}}(\mathbf{r})$, calculated in the Thomas Fermi limit, is equal to $gn(\mathbf{r})$ inside and to $V_{\mathrm{ext}}(\mathbf{r}) - \mu$ outside the condensate. At high q the main contribution to the dynamic structure factor (10) arises from the excited states with $\mathbf{p}_f \sim \mathbf{q}$. This has been taken into account in the eikonal correction $\tilde{u}(\mathbf{r})$ [second factor of Eq. (40)], where $\mathbf{p}_f$ was chosen along the x axis, i.e., the axis fixed by the vector $\mathbf{q}$. Notice that in the eikonal approximation the free-particle solution $e^{i\mathbf{p}_f \cdot \mathbf{r}/\hbar}$ is modified by the interactions only through a change of the phase. The importance of such a correction in the behavior of the dynamic structure factor depends on the maximum phase deviation of $u(\mathbf{r})$ from a pure plane wave, which is determined by the Born parameter b

$$b = \frac{\mu}{E_{\mathrm{r}}} \frac{qR_\perp}{\hbar}, \tag{41}$$

where $E_{\mathrm{r}} = q^2/2m$ and $R_\perp$ is the Thomas-Fermi radius (31). Different from the ratio μ/E_{r}, the Born parameter depends explicitly on the size of the atomic cloud.

From Eq. (6) one gets, in first approximation,

$$v(\mathbf{r}) \simeq -\frac{mgn(\mathbf{r})}{p_f^2} u(\mathbf{r}). \tag{42}$$

Notice that inclusion of $v(\mathbf{r})$ in Eq. (5) for $u(\mathbf{r})$ would result in a higher order correction. Making the transformation $\mathbf{p}_f = \mathbf{p} + \mathbf{q}$, the dynamic structure factor (10) takes the form:

$$S(\mathbf{q},E) = \int d\mathbf{p} |M|^2 \delta\left(E - \frac{q^2}{2m} - \frac{qp_x}{m} \right), \tag{43}$$

with

$$M = \frac{1}{(2\pi\hbar)^{3/2}} \int d\mathbf{r} \psi_0(\mathbf{r}) \exp\left[i \frac{m}{\hbar q} \int_0^x dx' V_{\mathrm{eff}}(x',y,z) \right] \times \left(1 - \frac{gn(\mathbf{r})}{q^2/m} \right) \exp\left[-i \left(\frac{\mathbf{p} \cdot \mathbf{r}}{\hbar} \right) \right], \tag{44}$$

where we have approximated $p_f \sim q$ in the evaluation of $v(\mathbf{r})$ and in the eikonal correction and neglected the kinetic energy term $p^2/2m$ in the argument of the δ function. This is a very accurate approximation if one works with large samples, where the Thomas-Fermi approximation $\psi_0(\mathbf{r}) = \sqrt{[\mu - V_{\mathrm{ext}}(\mathbf{r})]/g}$ applies.

If the Born parameter (41) is small, then the eikonal correction can be neglected and, ignoring the small term $gn(\mathbf{r})m/q^2$ in Eq. (44), one recovers the IA result (3). Conversely, if b is large one finds a different behavior. In this case the main contribution to the double integral $|M|^2$ arises from the region where $|x_1 - x_2| \sim R_\perp/b \ll R_\perp$ and the eikonal correction to the relative phase $(m/\hbar q)\int_{x_2}^{x_1} dx' V_{\mathrm{eff}}(x',y,z)$ can be consequently written as $(m/\hbar q) V_{\mathrm{eff}}(x,y,z)(x_1 - x_2)$, with $x = (x_1 + x_2)/2$. In these expressions we have set $y_1 = y_2 = y$ and $z_1 = z_2 = z$ as a consequence of the integration on p_y and p_z in Eq. (43). By integrating with respect to the relative variable $x_1 - x_2$ and to p_x one finally recovers the LDA result (15) for large q, where $\epsilon(\mathbf{q},\mathbf{r}) \simeq q^2/2m + gn(\mathbf{r})$. In conclusion the eikonal approximation (43)–(44) provides the proper description of the dynamic structure factor in the Thomas-Fermi limit in all the regimes of momentum transfer ranging from the LDA to the IA, provided $\mu \ll E_{\mathrm{r}}$. It is interesting to notice that the Born parameter (41) fixes also the ratio between the widths (25) and (34) of the dynamic structure factor calculated in the IA and LDA limits, respectively. In fact one has

$$\frac{\Delta_{LDA}}{\Delta_{IA}} = \frac{b}{14}, \tag{45}$$

so that the comparison between the two widths provides an equivalent criterion for the applicability of the two opposite approximations. The transition between the LDA and the IA takes place when the ratio (45) is close to unity. Using the relation $\mu = \hbar^2/2m\xi^2$, where ξ is the healing length (12) calculated at the center of the trap, this corresponds to the value $q = \hbar R_\perp/14\xi^2$ for the momentum transfer. Notice that this value is much larger than the inverse of ξ, since in the

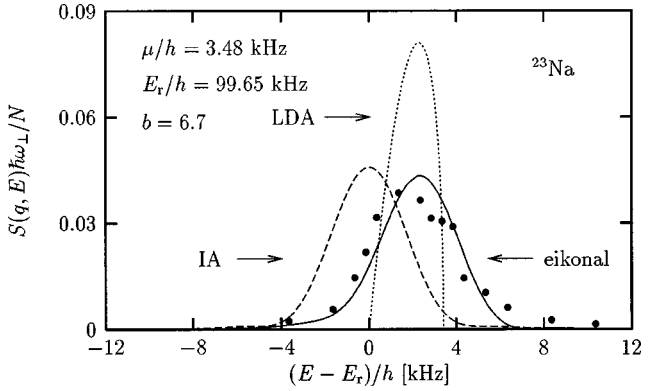

FIG. 5. Dynamic structure factor of a trapped Bose condensate at $T=0$. The numerical predictions of the eikonal approximation (solid curve), IA (dashed curve), and LDA (dotted curve) are compared with the experimental data of Ref. [4], normalized to reproduce $S(q)=1$. The momentum transfer is taken along the x axis. The trap parameters are the same as in Fig. 4.

Thomas-Fermi regime $R_\perp \gg \xi$ (see also Fig. 9). For example, in the cloud of sodium atoms explored in Ref. [4] with peak density $n(0)=3.8\times10^{14}$ cm^{-3}, corresponding to $b\simeq14$, one has $1/R_\perp\simeq0.1$ μm^{-1}, $1/\xi\simeq5$ μm^{-1}, and $R_\perp/14\xi^2 \simeq 20$ μm^{-1}.

Equations (43)–(44) can be easily calculated numerically in all the regimes between the LDA and the IA. The comparison with the available experimental results (see Fig. 5) is rather good and explains the deviation of the observed signal from the LDA as well from the IA predictions. The width of the dynamic structure factor in general is well reproduced by the quadrature expression $\sqrt{\Delta_{LDA}^2+\Delta_{IA}^2}$ accounting for both the LDA and the IA widths (see also [23]).

IV. SUM RULES

The conditions of applicability of the local density and impulse approximations presented in the previous section can also be discussed using a sum rule approach [24], which allows for an exact determination of the width of the dynamic structure factor in some relevant limiting cases.

We have already introduced in the previous section the moments of the dynamic structure factor relative to the operator $\rho_{\mathbf{q}}$. In terms of the matrix elements $\langle n|\rho_{\mathbf{q}}|0\rangle$ of the density operator one can write

$$m_k(\mathbf{q})=\sum_{n\neq0}|\langle n|\rho_{\mathbf{q}}|0\rangle|^2(E_n-E_0)^k=\int_{0^+}^{\infty}dES(\mathbf{q},E)E^k, \tag{46}$$

and, using the closure relationship $\Sigma_n|n\rangle\langle n|=\mathbf{1}$, one can easily express the moments $m_k(\mathbf{q})$ in terms of the mean values of commutators between the Hamiltonian and the operator $\rho_{\mathbf{q}}$ on the ground state $|0\rangle$. Using the property $S(\mathbf{q},E)=S(-\mathbf{q},E)$, holding in the presence of parity or time-reversal invariance, we find the following results for the lowest moments:

$$m_0(q)=\langle\rho_{\mathbf{q}}^\dagger\rho_{\mathbf{q}}\rangle-|\langle\rho_{\mathbf{q}}\rangle|^2=NS(q), \tag{47}$$

$$m_1(q)=\frac{1}{2}\langle[\rho_{\mathbf{q}}^\dagger,[H,\rho_{\mathbf{q}}]]\rangle=N\frac{q^2}{2m}, \tag{48}$$

$$m_2(q)=\langle[\rho_{\mathbf{q}}^\dagger,H][H,\rho_{\mathbf{q}}]\rangle=N\left[[2-S(q)]\left[\frac{q^2}{2m}\right]^2+\frac{\hbar^2q^2}{m^2}D^x(q)\right], \tag{49}$$

$$m_3(q)=\frac{1}{2}\langle\{[\rho_{\mathbf{q}}^\dagger,H],[H,[H,\rho_{\mathbf{q}}]]\}\rangle=N\left[\left[\frac{q^2}{2m}\right]^3+4\left[\frac{q^2}{2m}\right]^2\left(3\frac{E_{\rm kin}^x}{N}+\frac{E_{\rm int}}{N}\right)+\frac{q^2}{2m}\frac{\hbar^2}{m}\langle\partial_x^2V_{\rm ext}\rangle\right], \tag{50}$$

where we took the vector $\mathbf{q}$ along the x axis. Notice that in Eq. (47) we have subtracted the elastic contribution $|\langle\rho_{\mathbf{q}}\rangle|^2$. The kinetic structure function $D^x(q)$ is defined by

$$D^x(q)=\frac{1}{N}\int d\mathbf{r}_1d\mathbf{r}_2\cos[q(x_1-x_2)]\times\nabla_1^x\nabla_2^x\rho^{(2)}(\mathbf{r}_1,\mathbf{r}_2;\mathbf{r}_1',\mathbf{r}_2')|_{\mathbf{r}_1=\mathbf{r}_1',\mathbf{r}_2=\mathbf{r}_2'}, \tag{51}$$

where

$$\rho^{(2)}(\mathbf{r}_1,\mathbf{r}_2;\mathbf{r}_1',\mathbf{r}_2')=N(N-1)\int d\mathbf{r}_3d\mathbf{r}_4\cdots d\mathbf{r}_N\psi^*(\mathbf{r}_1,\mathbf{r}_2,\ldots,\mathbf{r}_N)\times\psi(\mathbf{r}_1',\mathbf{r}_2',\mathbf{r}_3,\mathbf{r}_4,\ldots,\mathbf{r}_N) \tag{52}$$

is the two-body density matrix. In the asymptotic limit $q\to\infty$ this function is related to the kinetic energy of the system [25]:

$$\lim_{q\to\infty}D^x(q)=\frac{2m}{\hbar^2}\frac{E_{\rm kin}^x}{N}. \tag{53}$$

The m_3 sum rule (50) has been obtained evaluating the commutators with the effective Hamiltonian

$$H=\sum_i\left[\frac{p_i^2}{2m}+V_{\rm ext}(\mathbf{r}_i)\right]+g\sum_{i<j}\delta(\mathbf{r}_i-\mathbf{r}_j), \tag{54}$$

and using the corresponding ground state of Gross-Pitaevskii theory. In particular $E_{\rm int}=g\int d\mathbf{r}n(\mathbf{r})^2/2$ corresponds to the expectation value of the two-body interaction energy.

The f-sum rule (48) is model independent [26] and is satisfied by both the LDA and IA as can be explicitly shown by integrating the corresponding dynamic structure factors. The other sum rules are instead correctly reproduced only in suitable ranges of momenta, which thereby provide the corresponding regimes of applicability of the two approximations.

The non-energy-weighted sum rule (47) coincides with the inelastic static structure factor $S(\mathbf{q})$, a quantity of high interest, directly related to the Fourier transform of the diagonal two-body density matrix:

$$S(\mathbf{q})=1+\frac{1}{N}\int d\mathbf{r}_1 d\mathbf{r}_2 e^{i\mathbf{q}\cdot(\mathbf{r}_1-\mathbf{r}_2)}[\rho^{(2)}(\mathbf{r}_1,\mathbf{r}_2;\mathbf{r}_1,\mathbf{r}_2) - n(\mathbf{r}_1)n(\mathbf{r}_2)]. \tag{55}$$

The LDA prediction for $S(\mathbf{q})$ has been already discussed in the previous section [see Eq. (20)]. This prediction is expected to hold in all regimes of small and high q except, of course, when $qR<\hbar$. In fact the static structure factor $S(\mathbf{q})$ is not sensitive to the Doppler broadening, which instead affects other moments of the dynamic structure factor. An interesting property of the static structure factor is the occurrence of a $1/q^2$ correction to the large q asymptotic value:

$$S(q)=1-\frac{8}{7}\frac{m\mu}{q^2}. \tag{56}$$

Such a law holds for $q\xi\gg\hbar$, but still in the Bogoliubov regime $qa\ll\hbar$, and is a peculiarity of dilute Bose gases [15], related to the shift of the average excitation energy given by the Feynman ratio $m_1/m_0=E_r+4\mu/7$. This behavior is not exhibited by dense liquids, like ^{4}He, where a and ξ are of the same order. The IA does not instead predict any q dependence for the static form factor and consequently fails in reproducing the shift of the peak.

The m_2 sum rule is also interesting for understanding the difference between the LDA and the IA. For large q this sum rule contains two corrections to the leading asymptotic value:

$$\lim_{q\to\infty} m_2(q)=\left[\frac{q^2}{2m}\right]^2+\frac{q^2}{2m}\left[\frac{4}{7}\mu+4\frac{E^x_{\rm kin}}{N}\right]. \tag{57}$$

The first correction, fixed by the chemical potential, arises again from the large q behavior (56) of $S(q)$ which, enters the expression (49) for m_2. The second contribution, proportional to the kinetic energy, arises form the kinetic structure factor $D^x(q)$. The first correction is correctly given by the LDA, the latter by the IA. It is worth noticing that if one calculates the rms width (22) only the kinetic energy term survives in the large q limit. This confirms the correctness of the impulse approximation in reproducing the width of the dynamic structure factor at high q.

Finally the m_3 sum rule is interesting because it can be explicitly evaluated for any value of q. For a uniform gas ($V_{\rm ext}=0$ and $E_{\rm kin}=0$) the ratio $\sqrt{m_3/m_1}$ coincides with the Bogoliubov excitation spectrum (11). In the presence of harmonic trapping it is instructive to calculate Eq. (50) in the small momentum transfer limit, where only the last term, containing the external potential, survives and the ratio $\sqrt{m_3/m_1}$ coincides with the frequency $\omega_\perp$ of the dipole mode. Indeed, the dipole mode is the only mode excited by the density operator $\rho_{\mathbf{q}}=\Sigma_j e^{i\mathbf{q}\cdot\mathbf{r}_j/\hbar}$ in the $q\to 0$ limit.

Before concluding this section we stress that the results discussed above hold in the Bogoliubov regime $qa\ll\hbar$. For larger momenta, relevant, for example, in the case of superfluid helium, a different behavior takes place. For example, result (56) for the static structure factor $S(q)$ is no longer valid. Particular attention should be also paid to the kinetic energy, which characterizes the large q behavior of m_2 and hence of the rms width. One should in fact distinguish between the kinetic energy of the condensate and the full kinetic energy of the system, which, even in dilute Bose gases, is dominated at $T=0$ by the high momentum components of $n(\mathbf{p})$. The former is given by (36) and becomes smaller and smaller as R increases. The latter is instead of the order of the interaction energy and would determine the rms width of the dynamic structure factor for momentum transfer larger than $\hbar/a$.

V. SCALING AND IMPULSE APPROXIMATION

In the previous sections we have often referred to the impulse approximation as the proper theory to describe the high-q response of the system. At the same time we have pointed out that the IA does not account for the mean field shift (23) of the peak energy occurring at high q, which is instead correctly predicted by the LDA. In this section we discuss in what sense the IA provides the exact asymptotic description of the dynamic structure factor. The discussion is simplified by using scaling, a concept already employed in other many-body systems, including atomic nuclei [27], liquids, and solids [28,2]. Let us introduce the scaling variable

$$Y=\frac{m}{q}\left(E-\frac{q^2}{2m}\right), \tag{58}$$

which is the relevant variable to describe the asymptotic behavior of the dynamic structure factor. We define the scaling function $F_0(Y)$ according to the asymptotic behavior

$$F_0(Y)=\lim_{q\to\infty}\frac{q}{m}\frac{S(\mathbf{q},E)}{N}, \tag{59}$$

where, in the limit, the excitation energy E varies with q in order to keep the value of Y fixed. Comparison with Eq. (28) shows that $F_0(Y)$ coincides with the longitudinal momentum distribution

$$F_0(Y)=\frac{1}{N}\int dp_y dp_z n(Y,p_y,p_z). \tag{60}$$

In terms of the scaling function $F_0(Y)$ the rms width takes the form

$$\Delta_{\rm rms}=\frac{q}{m}\sqrt{\int_{-\infty}^{\infty} dY F_0(Y)Y^2}. \tag{61}$$

Furthermore one has $\int_{-\infty}^{\infty} dY F_0(Y)=1$, and $\int_{-\infty}^{\infty} dY Y F_0(Y)=0$.

The scaling result (59)–(60) holds for a wide class of many-body systems interacting with realistic two-body potentials, and is not restricted to dilute gases (see, for example [29], and references therein). This means that corrections to the IA, due to final state interactions, give a vanishing contribution to the limit (59). In general the following expansion holds:

$$\frac{q}{m}\frac{S(\mathbf{q},E)}{N}=F_0(Y)+\frac{m}{q}F_1(Y)+\left(\frac{m}{q}\right)^2F_2(Y)+\cdots. \tag{62}$$

In the presence of parity or time-reversal symmetry the scaling function $F_0(Y)$ is symmetric: $F_0(Y)=F_0(-Y)$. Conversely one has $F_1(Y)=-F_1(-Y)$. This suggests that the proper symmetrization $[S(\mathbf{q},E)+S(\mathbf{q},2E-E_r)]/2$ of the measured signal with respect to the recoil energy $E_r=q^2/2m$ would ensure a faster convergence to the scaling limit [28]. From an experimental point of view the direct verification of scaling, by changing q and E keeping Y fixed, is likely the safest criterion for checking the achievement of the IA regime. A peculiarity of dilute gases is that it is possible to reach the scaling regime for values of momenta where the Bogoliubov theory is still applicable.

For a trapped Bose gas, the eikonal Eqs. (43)–(44) can be easily expanded for small values of the Born parameter (41), corresponding to high values of $q(b=2m\mu R_\perp/\hbar q)$. One finds

$$\frac{q}{m}\frac{S(\mathbf{q},E)}{N}=\frac{R_\perp}{\hbar}[f_0(y)+bf_1(y)+\cdots], \tag{63}$$

where $f_0(y)$ and $f_1(y)$ are dimensionless functions of the variable $y=(R_\perp/\hbar)Y$, directly related to the scaling functions of Eq. (62): $F_0(Y)=R_\perp f_0(y)/\hbar$ and $F_1(Y)=qR_\perp bf_1(y)/m\hbar$. The function $f_0(y)$ is given by

$$f_0(y)=\frac{15}{16}\int d\tilde{p}_y d\tilde{p}_z\left[\frac{J_2(\sqrt{y^2+\tilde{p}_y^2+\tilde{p}_z^2})}{y^2+\tilde{p}_y^2+\tilde{p}_z^2}\right]^2, \tag{64}$$

and is shown in Fig. 6 together with the Gaussian expansion

$$f_0(y)\simeq\frac{15\pi}{192}\exp\left[-\frac{3}{16}y^2\right], \tag{65}$$

yielding the results (33)–(34) for the dynamic structure factor. The function $f_1(y)$ is given by

$$f_1(y)=\frac{15}{2}\int_0^\infty dp_\perp p_\perp\frac{J_2(\sqrt{y^2+p_\perp^2})}{y^2+p_\perp^2}\int_0^1 dr_\perp r_\perp J_0(r_\perp p_\perp)\times\int_0^{\sqrt{1-r_\perp^2}}dx\sqrt{1-x^2-r_\perp^2}\sin(yx)x\left(1-\frac{x^2}{3}-r_\perp^2\right), \tag{66}$$

and is also shown in Fig. 6.

Starting from Eq. (63) one can evaluate the shift of the peak with respect to the recoil energy E_r due to the first correction to the IA. Imposing the condition $\partial_E S(\mathbf{q},E)=0$ one finds, after some straightforward algebra, $E_{peak}=E_r+2\mu/3$, showing that result (24) for the line shift holds not only in the high-q LDA regime where b is large, but also for small values of b. This behavior is not obvious and seems to suggest that the same result holds also for intermediate values of b.

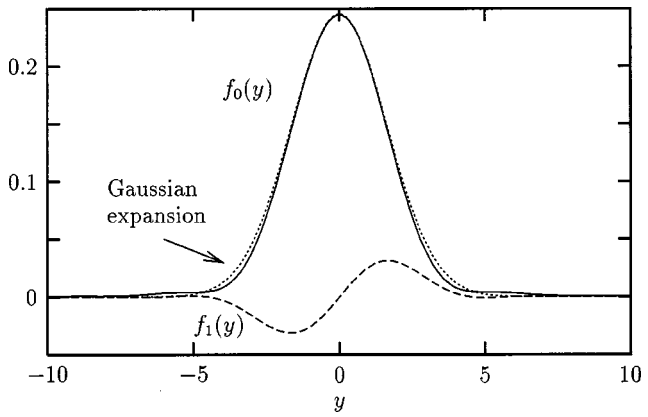

FIG. 6. Dimensionless scaling functions in the Thomas-Fermi regime: the $f_0(y)$ function [Eq. (64)] (solid line) is compared with its Gaussian expansion (65) (dotted line). The function $f_1(y)$ [Eq. (66)] is also shown (dashed line).

VI. DYNAMIC STRUCTURE FACTOR AND VORTICES

The study of vortices in trapped Bose gases is presently a challenging topic of both theoretical and experimental investigation. First experimental evidence of vortices has been recently reported [30,31]. On the theoretical side the structure of vortices, the corresponding stability conditions, as well as their consequences on the dynamic behavior of the condensate have already attracted the attention of many physicists. The identification of suitable methods of detection has also been the object of theoretical investigation. These include the expansion of the condensate [32], the shift of the collective excitation frequencies [33], and the occurrence of dislocations in the interference patterns [34].

In this section we show that the measurement of the dynamic structure factor in the IA regime would represent a powerful tool to reveal vortices in a trapped Bose gas. In fact a vortex strongly affects the momentum distribution of the system. This can be easily understood by noting that the kinetic energy of a trapped condensate is roughly doubled by the addition of a vortex [19].

In the presence of a quantized vortex aligned along the z axis the wave function of the condensate takes the form

$$\psi(\mathbf{r})=e^{i\varphi}\psi_0(r_\perp,z), \tag{67}$$

where $\psi_0(r_\perp,z)$ is the solution of the Gross-Pitaevskii equation [8,35]

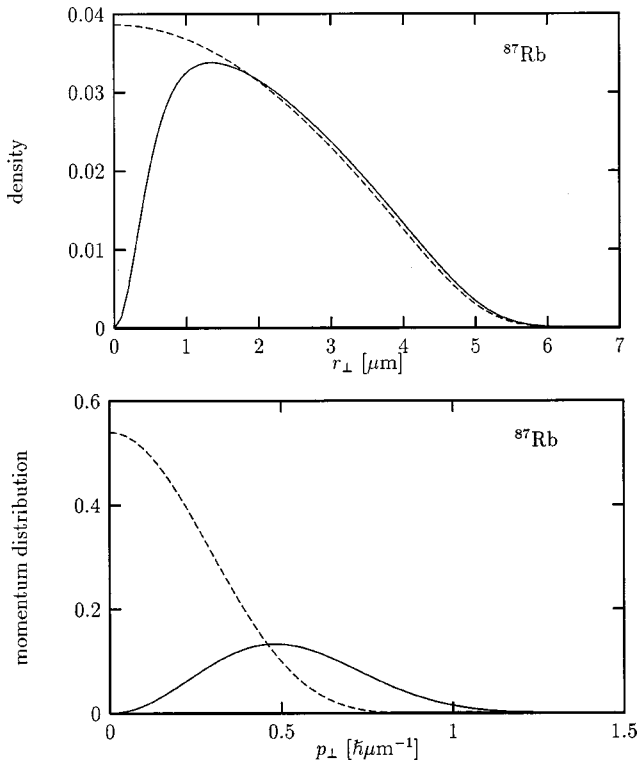

FIG. 7. Density profile (up) and momentum distribution (down) of a trapped Bose condensate as a function of the radial variables $r_\perp$ and $p_\perp$, integrated along z and p_z, respectively, in the absence (dashed line) and in the presence of a quantized vortex (full line). These profiles correspond, in the absence of the vortex, to a central density $n(0)\simeq 1\times 10^{14}$ cm^{-3}. The trap parameters are $\omega_z = 2\pi 220$ Hz, and $\lambda=\sqrt{8}$.

$$\left[-\frac{\hbar^2\nabla^2}{2m} + \frac{\hbar^2}{2mr_\perp^2} + \frac{m}{2}(\omega_\perp^2 r_\perp^2 + \omega_z^2 z^2) + g\psi_0(r_\perp,z)^2 \right] \psi_0(r_\perp,z) = \mu\psi_0(r_\perp,z), \qquad (68)$$

which contains the additional centrifugal term $\hbar^2/2mr_\perp^2$. Solutions of Eq. (68) have been obtained numerically in [36]. The density distribution $|\psi_0(r_\perp,z)|^2$ exhibits a hole whose size is of the order of the healing length (12) of the gas ξ, which, in the Thomas-Fermi limit, is much smaller than the size of the condensate. Also in momentum space the distribution exhibits a hole as shown in Fig. 7. This is the consequence of the phase in Eq. (67), which gives a vanishing value to the integral (29) at $p_\perp=0$, where $p_\perp$ is the radial component of the momentum vector **p**. The size of the hole is of the order of $\hbar/R_\perp$, and consequently comparable to the total size of the condensate in momentum space. This can be easily seen calculating the momentum distribution in the Thomas-Fermi limit. In this limit the main effect of the vortex on the momentum distribution arises from the phase $e^{i\varphi}$, and one can safely use for ψ_0 the Thomas-Fermi expression $\sqrt{[\mu - V_{\rm ext}(\mathbf{r})]/g}$, holding in the absence of the vortex. The result for $n(\mathbf{p})$ can then be written in the form

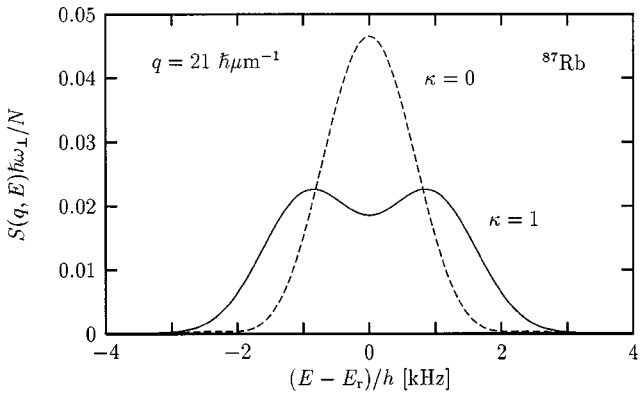

FIG. 8. Dynamic structure factor of a rubidium-trapped Bose condensate at $T=0$ in the presence (solid line) and in the absence (dashed line) of the vortex, calculated using the impulse approximation (3). The momentum transfer is taken along the x axis. The trap parameters are the same as in Fig. 7.

$$n_{\rm TF}(\mathbf{p}) = N\frac{R_\perp^3}{\hbar}\frac{15}{16}\frac{\lambda}{\pi^4}\left| \int_0^{2\pi} d\varphi e^{i\varphi} \int_0^1 dr_\perp r_\perp \int_0^{\sqrt{1-r_\perp^2}} dz \times e^{i\tilde{\mathbf{p}}\cdot\mathbf{r}}\sqrt{1-r_\perp^2-z^2} \right|^2, \qquad (69)$$

where $\tilde{\mathbf{p}}$ is the scaled momentum vector $\tilde{\mathbf{p}} \equiv (p_x,p_y,p_z/\lambda)R_\perp/\hbar$, already introduced in Sec. III B. Notice that in the Thomas-Fermi limit the effect of the vortex is factorized through a dimensionless integral.

In Fig. 8 we report the dynamic structure factor calculated in the IA [see Eq. (3)] with and without the vortex. The calculation was carried out for a gas of $N=10^4$ ^{87}Rb atoms trapped in a disk-type geometry ($\lambda=\sqrt{8}$). For this low density sample the IA is very accurate. The double peak structure in $S(\mathbf{q},E)$ reflects the occurrence of a peculiar Doppler effect, and represents a clear signature of the vortex. In fact the vortex generates a velocity field in the condensate with significant components both parallel and antiparallel to the momentum transfer **q**.

Another important example where the investigation of the dynamic structure factor can provide useful informations on coherence phenomena is the study of interference effects in momentum space. This possibility was recently discussed in Ref. [37], where two identical spatially separated condensates were considered. The momentum distribution of such a configuration exhibits interference patterns and gives rise to characteristic fringes in the shape of the dynamic structure factor. At high q, where one can use the IA, one finds [37]

$$S(\mathbf{q},E) = 2S_0(\mathbf{q},E)\left[1+\cos\left(\frac{Yd}{\hbar}+\varphi\right)\right], \qquad (70)$$

where $S_0(\mathbf{q},E)$ is the dynamic structure factor of the single condensate, Y is the scaling variable (58), φ is the relative phase between the two condensates, and d is their spatial separation. The frequency period of the fringes is $\Delta\nu$

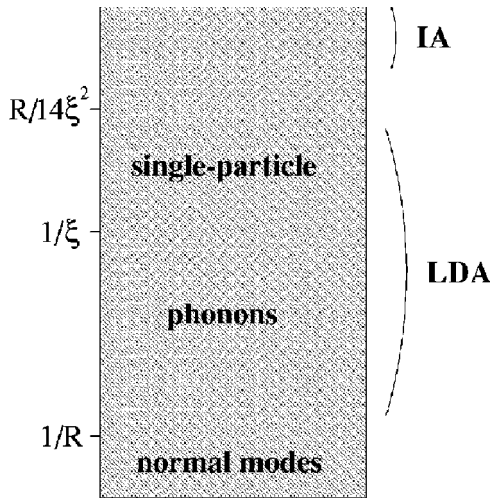

FIG. 9. Relevant wave vector regimes characterizing the dynamic structure factor at $T=0$. R is the size of the condensate (31); ξ is the healing length (12). The ranges of applicability of the local density approximation (LDA) and of the impulse approximation (IA) are also schematically indicated. The momentum transfer $\hbar R/14\xi^2$ corresponds to the condition $\Delta_{LDA}=\Delta_{IA}$ for the LDA and IA widths of the dynamic structure factor [see Eq. (45)].

$=\Delta E/h=q/md$. By choosing $q\simeq 20\hbar\ \mu\mathrm{m}^{-1}$ and $d\simeq 35\ \mu$m the fringes turn out to be ~ 1.5 kHz, for a sodium sample.

VII. CONCLUSIONS

In this paper we have provided a theoretical discussion of the dynamic structure factor $S(\mathbf{q},E)$ of a trapped Bose-Einstein condensate at low temperature. A first important aim was the development of the proper many-body formalism, based on Bogoliubov theory, to describe in a quantitative way the several interesting features exhibited by $S(\mathbf{q},E)$. These mainly concern the role of two-body interactions, which sizably affect the response of the system in all the relevant regimes of momentum transfer. The possibility of providing accurate theoretical predictions for the dynamic structure factor is particularly appealing in view of the recent experimental data obtained via two-photon Bragg scattering. The available data are in general agreement with theory, and thereby provide a further important proof of the crucial role played by two-body interactions in these trapped Bose-Einstein condensed gases. Interactions affect the shape of $S(\mathbf{q},E)$ at both small momentum transfer, where they are responsible for the propagation of phonons, and at high momentum where they show up in the shift of the peak with respect to the free recoil energy $q^2/2m$ as well as in the width, which is sensitive to both mean field and Doppler effects. Various approximate schemes have been considered in order to better discuss the main physical features. These schemes are summarized in Fig. 9 where the importance of the characteristic length scales of the problem emerges clearly. At momentum transfer smaller than the inverse of the size of the system, the response is characterized by the discretized normal modes of the system. This regime has been already discussed in other works and has not been considered here. At higher momenta the system behaves locally as a uniform gas. This is the range of applicability of the local density approximation (LDA), which successfully describes the excitation of phonons as well as, at momenta larger than the inverse of the healing length, the corrections to the free-particle motion due to mean field interactions. At even higher momenta the response of the system can no longer be described locally, because it is sensitive to the momentum distribution of the condensate, a quantity associated with long-range coherence effects. This regime is well described by the impulse approximation (IA), a theory currently employed to investigate the quasifree response of various many-body systems. In our work we have limited the use of the IA to momenta smaller than the inverse of the scattering length, i.e., to the range of applicability of Bogoliubov theory. In this regime only the momentum distribution of the condensate is relevant and one can safely ignore the higher momentum components of $n(\mathbf{p})$, which would be crucial to describe the response at momentum transfers larger than $\hbar/a$. An interesting feature emerging from our analysis is that the transition between the LDA and the IA regimes is characterized by an important physical parameter, the so-called Born parameter (41), which depends explicitly on the size of the system. The corresponding transition takes place at momenta fixed by the combination $\hbar R/\xi^2$. We have shown that the transition can be accounted for by an eikonal treatment of the solutions of the Bogoliubov equations, and a full calculation of $S(\mathbf{q},E)$ has been presented in this regime, showing good agreement with experiments. Many of the relevant features exhibited by the dynamic structure factor in these trapped Bose gases have been also presented and discussed using the formalism of sum rules and the concept of scaling.

A second important point emerging from our analysis was that the dynamic structure factor in the IA regime of high momentum transfer offers a new important investigation tool. Actually Bose-Einstein condensation in momentum space provides a deeper understanding of long-range coherence phenomena in comparison with the studies of the density profiles, which have been so far the main object of investigation. Quantized vortices provide a significant example in which the dynamic structure factor exhibits nontrivial features, reflecting the peculiar behavior of the phase of the order parameter. In particular the dynamic structure factor is characterized by a hole occurring at the recoil energy and whose size is comparable to the total width of the signal.

ACKNOWLEDGMENTS

We are very grateful to W. Ketterle and A. P. Chikkatur for many fruitful discussions and for providing experimental data and details. L.P. would like to acknowledge many discussions during the BEC workshop at The Aspen Center for Physics. D.M.S.-K. acknowledges support from Robert A. Millikan. This work has been supported by the Istituto Nazionale per la Fisica della Materia (INFM) through the Advanced Research Project on BEC, and by the Ministero dell'Università e della Ricerca Scientifica e Tecnologica (MURST).

[1] H. Palevski, K. Otnes, and K. E. Larson, Phys. Rev. **112**, 11 (1958); D. G. Henshaw and A. D. B. Woods, *ibid.* **121**, 1266 (1961).
[2] P. Sokol in *Bose-Einstein Condensation*, edited by A. Griffin, D. W. Snooke, and S. Stringari (Cambridge University Press, Cambridge, 1995), p. 51.
[3] L. Van Hove, Phys. Rev. **95**, 249 (1954).
[4] J. Stenger, S. Inouye, A. P. Chikkatur, D. M. Stamper-Kurn, D. E. Pritchard, and W. Ketterle, Phys. Rev. Lett. **82**, 4569 (1999).
[5] D. M. Stamper-Kurn, A. P. Chikkatur, A. Görlitz, S. Inouye, S. Gupta, D. E. Pritchard, and W. Ketterle, Phys. Rev. Lett. **83**, 2876 (1999).
[6] A. L. Fetter and J. D. Walecka, *Quantum Theory of Many-Particle Systems* (McGraw-Hill, New York, 1971).
[7] P. C. Hohenberg and P. M. Platzman, Phys. Rev. **152**, 198 (1966).
[8] L. P. Pitaevskii, Zh. Éksp. Teor. Fiz. **40**, 646 (1961) [Sov. Phys. JETP **13**, 451 (1961)].
[9] A. L. Fetter, Ann. Phys. (N.Y.) **70**, 67 (1972).
[10] Wen-Chin Wu and A. Griffin, Phys. Rev. A **54**, 4204 (1996).
[11] N. Bogoliubov, J. Phys. (Moscow) **11**, 23 (1947).
[12] E. Timmermans and P. Tommasini, e-print cond-mat/9707322.
[13] F. Dalfovo, S. Giorgini, L. Pitaevskii, and S. Stringari, Rev. Mod. Phys. **71**, 463 (1999).
[14] In the presence of harmonic trapping the static structure factor of an ideal Bose gas is actually given by $S(q)=1-\exp[-q^2/(\hbar m\omega_z)]$, and vanishes when $q\rightarrow 0$. For the values of q employed in the experiment of [5] the prediction of the ideal Bose gas model is, however, always close to 1.
[15] K. Huang, *Statistical Mechanics*, 2nd ed. (Wiley, New York, 1978).
[16] G. Baym and C. Pethick, Phys. Rev. Lett. **76**, 6 (1996).
[17] F. Dalfovo, L. Pitaevskii, and S. Stringari, Phys. Scr., T **66**, 234 (1996).
[18] F. Dalfovo, L. Pitaevskii, and S. Stringari, Phys. Rev. A **54**, 4213 (1996).
[19] E. Lundh, C. J. Pethick, and H. Smith, Phys. Rev. A **55**, 2126 (1997).
[20] The coherence length should not be confused with the healing length ξ (12) which, different from χ_x, becomes small as the density of the sample increases.
[21] L. D. Landau and E. M. Lifshitz, *Quantum Mechanics*, 3rd ed. (Pergamon Press, Oxford, 1977), Sec. 131.
[22] The eikonal approximation has been successfully used for describing both electron-nucleus scattering and neutron scattering from liquid helium (see [38,29] and references therein).
[23] D. M. Stamper-Kurn, Ph.D. Thesis, 1999.
[24] E. Lipparini and S. Stringari, Phys. Rep. **175**, 103 (1989).
[25] E. Feenberg, *Theory of Quantum fluids* (Academic, New York, 1969), Chap. 4; D. Hall and E. Feenberg, Ann. Phys. (N.Y.) **63**, 335 (1971).
[26] D. Pines and P. Nozières, *The Theory of Quantum Liquids* (Benjamin, New York, 1966), Vol. I.
[27] D. Day, J. S. McCarthy, T. W. Donnelly, and I. Sick, Annu. Rev. Nucl. Part. Sci. **40**, 357 (1990).
[28] V. F. Sears, Phys. Rev. B **30**, 44 (1984).
[29] C. Carraro and S. E. Koonin, Nucl. Phys. A **524**, 201 (1991).
[30] M. R. Matthews, B. P. Anderson, P. C. Haljan, D. S. Hall, C. E. Wieman, and E. A. Cornell, Phys. Rev. Lett. **83**, 2498 (1999).
[31] K. W. Madison, F. Chevy, W. Wohlleben, and J. Dalibard, Phys. Rev. Lett. **84**, 806 (2000).
[32] E. Lundh, C. J. Pethick, and H. Smith, Phys. Rev. A **58**, 4816 (1998); F. Dalfovo and M. Modugno, *ibid.* **61**, 023 605 (2000).
[33] F. Zambelli and S. Stringari, Phys. Rev. Lett. **81**, 1754 (1998); A. A. Svidzinsky and A. Fetter, Phys. Rev. A. **58**, 3168 (1998).
[34] E. L. Bolda and D. F. Walls, Phys. Rev. Lett. **81**, 5477 (1998); J. Tempere and J. T. Devreese, Solid State Commun. **108**, 993 (1998).
[35] E. P. Gross, Nuovo Cimento **20**, 454 (1961).
[36] F. Dalfovo and S. Stringari, Phys. Rev. A **53**, 2477 (1996).
[37] L. P. Pitaevskii and S. Stringari, Phys. Rev. Lett. **83**, 4237 (1999).
[38] S. A. Gurvitz and A. S. Rinat, Phys. Rev. C **47**, 2901 (1993).